Available online at www.sciencedirect.com
SCIENCE DIRECT®
International Journal of Heat and Mass Transfer 48 (2005) 1505–1517
International Journal of HEAT and MASS TRANSFER
www.elsevier.com/locate/ijhmt

Heat transfer from a cylinder in axial turbulent flows

Roland Wiberg [a], Noam Lior [b,*]

[a] Department of Mechanics/FaxénLaboratoriet, KTH, SE-100 44 Stockholm, Sweden
[b] Department of Mechanical Engineering and Applied Mechanics, University of Pennsylvania, 297 Towne Building, 220 South 33rd Street, Philadelphia, PA 19104-6315, USA

Received 12 March 2004; received in revised form 15 October 2004
Available online 22 December 2004

Abstract

Local convective heat transfer coefficients were measured on a two-diameter long cylinder in axial flows of air at conditions unexplored so far, by using thermochromic liquid crystals (TLC) coated on an electrically heated strip-foil consisting bonded to the external surfaces. The Reynolds numbers (Re) based on the cylinder diameter were between 8.9×10^4 and 6.17×10^5, and the flow in front of the cylinder was modified in some cases by the use of a turbulence generating grid, or by circular disc inserts of two sizes placed upstream of the cylinder. These created a major change in the local convective heat transfer coefficient distribution on the cylinder. Increase of the turbulence intensity from $Tu < 0.1\%$ to $Tu = 6.7\%$ at the same Re increased the average calculated Nusselt number Nu over the cylinder by 25%, and decreased the Nu non-uniformity over the surface. One of the flow modification inserts also reduced significantly the Nu non-uniformity. The position of flow reattachment was measured using tufts. Our heat transfer data agree well with the small amount if data published of others, when extrapolated to their conditions. Correlations between the Nu and Re in the form $Nu = CRe^e$ were established and presented for the average Nu on the front, middle and rear cylinder surfaces, and the variation of the local exponent e was shown along the cylinder. Introducing a new technique, a TLC-coated heated flat plate mounted in the flow above the cylinder in the meridional plane was demonstrated to help visualize the flow field above the cylinder. A track of maximum convective coefficients on this plate was found similar in position to the stream line dividing the forward and backward flows in a case measured for the separated flow in a past study.

Keywords: Circular cylinder; Axial flow; Convective heat transfer; Thermochromic liquid crystals; Separated flows

1. Introduction

It is of interest to know convection heat transfer coefficient (or Nusselt number) distributions over surfaces of blunt bodies in high speed flow in many diverse applications, including cooling of electronic equipment, cooling or heating of foodstuffs, and gas-cooled quenching. The latter was a topic of extensive study at the FaxénLaboratoriet of the Royal Institute of Technology, Sweden [1–7].

In quenching, the product hardness, uniformity of mechanical properties, and shape distortion depend on the rate and uniformity of the cooling. Gas quenching requires high gas speeds and pressures (typical values

* Corresponding author. Tel.: +1 215 898 4803; fax: +1 215 573 6334.
E-mail addresses: roland@mech.kth.se (R. Wiberg), lior@seas.upenn.edu (N. Lior).

0017-9310/$ - see front matter © 2004 Elsevier Ltd. All rights reserved.
doi:10.1016/j.ijheatmasstransfer.2004.10.015

Nomenclature

a, b, c, d, e, f	positions on the cylinder
D	outer diameter of the cylinder
h	local convective heat transfer coefficient, $W\,m^{-2}\,K^{-1}$
$\overline{h}$	surface averaged convective heat transfer coefficient
k	heat conductivity, $W\,m^{-1}\,K^{-1}$
L	length of the cylinder
Nu	local Nusselt number (Eq. (3)), dimensionless
$\overline{Nu}$	surface average of Nu, dimensionless
Nu_{max}, Nu_{min}	extremes values of Nu along a–d, dimensionless
R	outer radius of the cylinder
r	radius
Re	Reynolds number (Eq. (1)), dimensionless
T	temperature
TLC	thermochromic liquid crystals
Tu	free stream turbulence (Eq. (5)), dimensionless
U	time-averaged air velocity (in x-direction), ms^{-1}
u'	the fluctuating component of the air velocity (x-direction), ms^{-1}
q''	electrically supplied surface heat flux, $W\,m^{-2}$
x, y	coordinates

Greek symbols

v	kinematic viscosity, $m^2\,s^{-1}$
σ_{Nu}	surface weighted relative standard deviation in Nu, (Eq. (7)), dimensionless
σ_{max}	relative max–min difference in Nu, (Eq. (8)), dimensionless

Subscript

∞	for air at free stream conditions

are at least $10\,ms^{-1}$ and 10 bar, but they vary widely depending on the application), i.e. turbulent flows with Reynolds numbers typically between a few hundred thousand to a few million. The flows are thus highly turbulent, with separations and reattachments, which create significant convection heat transfer coefficient non-uniformity over the body surface. These coefficients must be controlled in magnitude and uniformity all over the surfaces to obtain optimal quench products.

In this paper we report on measurements of the temperature and Nusselt number distributions over the surfaces of a cylinder with a length to diameter ratio $LD^{-1} = 2.00$, in axial flows. This geometry is typical for short cylinders and many parts being quenched. The flows were in the Reynolds number range of $8.9 \times 10^4 < Re < 6.17 \times 10^5$, with the Reynolds number defined based on the cylinder diameter, as

$$Re = \frac{U_\infty D}{v_\infty} \tag{1}$$

where U_∞ and v_∞ is the velocity and the kinematic viscosity of the free stream air respectively.

The approaching flows investigated were a free stream (unmodified by upstream objects), and also flows affected by a turbulence-generating grid, and in some cases by flow modification inserts (circular discs) upstream of the cylinder. Information about the nature of the flow along the cylinder is also provided.

While there exists a fair number of experimental studies that provide Nusselt number distributions for single cylinders in cross-flow (cf. [8–10]) and multiple cylinders in cross-flow (cf. [11,12]), little information is available for cylinders in axial flow, and none were measured for $Re > 5.5 \times 10^4$.

In an experimental study of a cylinder in axial flow the mass transfer was measured over the cylinder upstream (front) surface by using the naphthalene sublimation technique, for $5 \times 10^3 < Re < 5 \times 10^4$ and at $Tu = 0.5\%$ [13]. Employing the mass–heat transfer analogy for air the average Nu over this surface is correlated, as

$$\overline{Nu} = 0.927 Re^{1/2} \tag{2}$$

where the local Nusselt number (Nu) is calculated as

$$Nu = \frac{hD}{k_\infty} \tag{3}$$

where k_∞ is the heat conductivity of the free stream air.

The local convection mass/heat transfer from this surface was found to increase from the center of the surface towards the outer radius, and was found to be 2.2 times higher at the edge than at the center, and independent of Re, indicating that Nu increased as $Re^{0.5}$ over the entire surface.

Measurements of Nu on the round surface of a cylinder, at constant surface heat flux, in axial flow, were performed for $2.52 \times 10^4 < Re < 5.36 \times 10^4$, $Tu = 0.8\%$ and $LD^{-1} = 13$ [14], and for $8 \times 10^3 < Re < 4.7 \times 10^4$, $Tu = 0.5\%$ and $LD^{-1} = 10$ [15]. In these studies, Nu was found to have a maximum at the distance $3R$ down-

stream from the front edge, then decreasing monotonically along the axis. For Re lower than 3.0×10^4 the maxima were found to occur somewhat closer to the front edge.

Velocity and turbulence measurements of the flow around a circular cylinder in an axial flow were performed for $Re = 2 \times 10^5$, $Tu < 0.2\%$, $LD^{-1} = 10$ [16]. In another study, Nu was measured for $4.08 \times 10^4 < Re < 6.8 \times 10^4$, $Tu = 0.8\%$, $LD^{-1} = 10$ [17]. These investigations showed that the flow separated at the front edge and reattached to the surface at or slightly downstream of the maximum in Nu.

Our paper also investigates the effects of circular discs inserted upstream of, and parallel to, the cylinder front on the flow and heat transfer over the cylinder in axial flow. No such studies were found in the literature, although an extensive investigation was performed on their influence on the drag coefficient, for $1 \times 10^5 < Re < 8 \times 10^5$ and including flow visualization [18]. An optimal choice of disc diameter ($0.75D$) and distance ($0.375D$) from the cylinder front, reduced the total drag coefficient for the cylinder front and disc together from 0.72 to 0.01, which is comparable to that for a body without flow separation. The results were found to be independent of the Reynolds number and the disc surface roughness. The same drag reduction was also found for a rough cylinder front surface, preventing laminar separation, when the front edge had a radius of $(1/4)R$.

2. The experimental method

A closed loop wind tunnel at KTH was used for the measurements (cf. [19]). It has a 7-m long, 800×1200 mm wide test section a glass window for visual access from outside, and a turbulence level $Tu < 0.1\%$ at the test section inlet, see Fig. 1. An opening slit in the roof downstream of the cylinder maintained the pressure atmospheric and the upstream flow velocities were in the range $U_\infty = 9$–$64\ \mathrm{ms}^{-1}$, and the air temperatures $T_\infty = 25$–$28\ ^\circ\mathrm{C}$, while the local cylinder surface temperatures were within $T = 36$–$63\ ^\circ\mathrm{C}$, which was within the active range of the thermochromic liquid crystals (TLC) used for its surface temperature measurements.

The convection heat transfer coefficient distribution on the cylinder surfaces was evaluated from the measured temperatures and calculated from Eq. (4),

$$h = \frac{q'' - 5.67 \times 10^{-8}(T^4 - T_\infty^4)}{T - T_\infty} \tag{4}$$

where the denominator is the cylinder surface convective heat flux composed of q'' (in $\mathrm{W\,m}^{-2}$), the constant heat flux generated electrically in a thin foil applied to the cylinder surface, reduced by the local heat radiation loss (typically 4–10% of q''). The latter was calculated assuming that the surface emittance = 1 (the test section walls were painted flat black) and with a radiative configuration factor of 1 for the exchange between the cylinder and the walls (because the cross-sectional area of the cylinder was only 2% of the wind tunnel cross-section). The temperatures in Eq. (4) are in K and the temperature of the test section walls was set to T_∞, justified by the relatively strong convective flow over the wooden walls, which tends to impart its own temperature to these walls. A similar procedure for correction of the radiative losses was used by Sparrow et al. [15].

2.1. The test cylinder

The test cylinder (Fig. 1) had a diameter of $D = 150$ mm and length of $L = 300$ mm, and was made of solid extruded polystyrene (EPS), which has a very

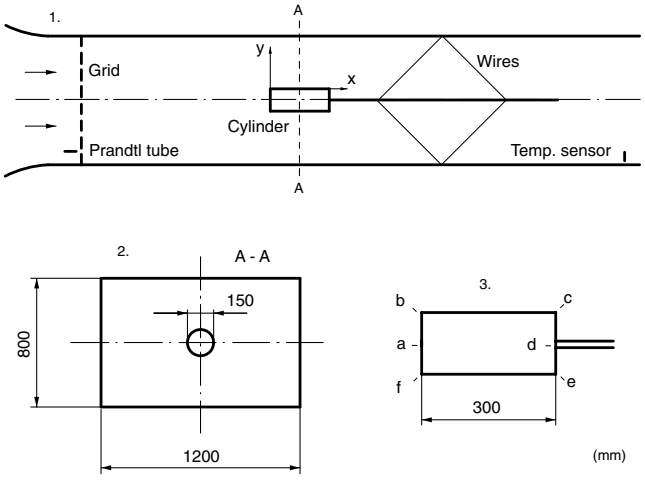

Fig. 1. The wind tunnel experimental setup. (1) The test section with the cylinder inside. (2) Cross-section of the test section. (3) The cylinder; points a, b, c, d, e, f serve to identify locations along it.

low heat conductivity ($k = 0.033\ \mathrm{W\,m^{-1}\,K^{-1}}$) to minimize heat transfer inside the cylinder. Three thermocouples were mounted just under the EPS surface along b–c at $xD^{-1} = 0.087$, 1.00 and 1.913, and along a–b, at the radius $rR^{-1} = 0.60$, using an adhesive to increase the thermal contact with the surface.

To make the cylinder surface smooth, a polyester film 125 μm thick ($k = 0.13\ \mathrm{W\,m^{-1}\,K^{-1}}$) was bonded on the EPS surface. An electrically conductive foil designed by us (manufactured by Calesco Foil AB [1]), was then bonded over the entire cylinder surface.

The foil was made of a thin layer of Inconel (12 μm thick, $k = 12\ \mathrm{W\,m^{-1}\,K^{-1}}$), chosen to reduce heat flux in the foil in directions parallel to its surface. A constant electrical surface power in the foil was ensured by letting the current flow in many 1.5 mm wide flat bands, which were spaced 0.2 mm apart and embedded in one of the faces of a 50 μm thick plastic polyimid film ($k = 0.12\ \mathrm{W\,m^{-1}\,K^{-1}}$). By dividing the foil electrically into 42 parts the uniformity was tested and the resistance was found to differ by only ±1.5% from the average. The variation in foil resistance with the temperature was low because of the low relative electrical resistance $1.25 \times 10^{-4}\ \mathrm{K^{-1}}$. Manually variable transformers (a.c.) supplied power to the foil within ±1.5% from the average.

Black paint and then the micro-encapsulated TLC of Hallcrest [2] type R35C20 C17-10 was sprayed on top of the foil in a 20 μm thick layer, in a 40 mm wide band along the cylinder line f–a–b–c–d (Fig. 1). This width was sufficient because of the axi-symmetry of the cylinder in the test section (as confirmed experimentally).

The possible conduction of heat inside the cylinder core and surface layers was examined with help of an one-dimensional calculation of the steady state heat conduction along the surface, using the thickness and the thermal conductivities of the layers and the TLC measured surface temperature field. Based on the measured time to reach the thermal steady state, and on the heat diffusivity of the EPS, the effective depth of the cylinder core, through which axial conduction took place, was estimated to be 14 mm. The axial heat flux loss in all the layers along the surface was then calculated to be within only 2% of the electrically supplied surface heat flux used in Eq. (4) for determining h. Larger losses may exist in the proximity of the edges, within a distance of $0.15R$. The foil was designed to supply no heat within a distance of $0.04R$ from the edges, and data from that zone were therefore not used.

[1] Calesco Foil AB, Västeråsvägen 9, S-73040 Kolbäck, Sweden.

[2] Hallcrest 20 Downing Road, West Meadows Industrial Estate, Derby DE21 6HA, UK.

To assist the detection of flow direction and behavior, 8 mm long thin soft cotton tufts were taped on the surface in a row, 90° away from the TLC band along the cylinder, 10 mm apart. The visual observations of the tufts to indicate the position of reattachment of the flow were performed at $Re = 1.75 \times 10^5$, while the cylinder was not heated.

A steel pipe $0.113D$ (17 mm) in diameter was bonded into the cylinder end, at the center, for support in the wind tunnel, and the pipe was held by eight 2.0 mm thick steel wires, which centered and aligned the cylinder to be parallel to the test section walls. Despite the rigid support, it was estimated that the cylinder vibrated with a displacement of about ±0.5 mm.

2.2. The measured flow configurations

The measurements were performed in four different configurations: (A) the cylinder alone in a low upstream turbulence flow, $Tu < 0.1\%$, (B) the cylinder in an upstream flow affected by turbulence-generating grid, $Tu = 6.7\%$, (C) the cylinder placed downstream of a circular disc $1/3D$ in diameter, which was centered on the cylinder axis, parallel to the cylinder front surface, and located at $xD^{-1} = -1.00$, (D) the cylinder placed downstream of a circular disc $(2/3)D$ in diameter, at the same position.

The turbulence-generating grid was made of square rods 10×10 mm, 50 mm apart, and was located upstream of the cylinder at $xD^{-1} = -5.50$ ($x = -825$ mm). Configurations (C) and (D) were included to examine the effects of upstream bodies on the convection heat transfer coefficients and flow on the cylinder, which also at least partially addresses the conditions when a body to be quenched is part of a multi-body quench-charge. The upstream discs in these configurations were $0.0333D$ (5 mm) thick with sharp corners and secured in their position by using 0.5 mm thick wires (in configuration (C): 5 or 6 wires, in configuration (D): 8 wires) fixed to the test section walls. The position of these wires was chosen so that their possible wakes would not directly affect the areas on the measured cylinder.

2.3. Calibration of the TLC

The TLC was calibrated before and after the measurements, in situ on the cylinder and inside the test section, using the thermocouples in the cylinder surface as reference. Color photographs of the TLC were taken through the glass window from a fixed position outside the test section using a Sony DCR-TRV 900E camera, 680×510 pixels, 24 bit color resolution, and two 24°, 50 W halogen lamps with built in IR and UV reduction filter fixed to the camera. The heating of the cylinder

surface from the lamps was measured to be <1% of the electrically supplied surface power of the foil.

The surface temperature was raised a few °C between each photography session, and the digital pictures were transferred from the camera to a Macintosh computer using fire wire (IEEE-1394). The image was then further loaded using QuickTime (an Apple Macintosh software) into Matlab5.2.1,™ [3] using its function *getvidframe*.

The color variable hue was calculated and related to the thermocouple measured temperatures, which were calibrated within ±0.1 °C against a Pt-100 resistance thermometer. Possible local non-uniformity in the TLC color (hue) response along the cylinder was investigated, using an isothermal chamber built for this purpose (having insulated walls of EPS, a fan, a heater and a window allowing photographs from outside). Based on the measured variation in hue along the cylinder, corrections were applied to the temperature–hue relation.

The position of the camera relative to the cylinder caused a varying pixel density in the image of the cylinder surface, which was corrected in the software. Many parameters affect a TLC temperature measurement, and further details of the TLC technique are given in [4]. All together, the errors in the local TLC measured surface temperatures were estimated to be within ±1.2 °C of the true surface temperatures.

2.4. The experimental procedure

The free stream flow velocity (measured using the Prandtl tube) and the flow temperature, were allowed to stabilize, U_∞ within ±0.5%, and T_∞ within ±0.1 °C. The heat flux q'' of the foil was increased until the surface temperatures came within the active temperature interval of the TLC and then stabilized typically over 10 min, within ±0.3 °C, as indicated by the thermocouples. In the steady state, color photographs of the TLC were taken, using the same camera, view angle, and light settings, as were used during the in situ calibrations. The electrical current to the heating foil was then shut off. This procedure was repeated for each measurement.

2.5. Turbulence measurements

The turbulence level (Tu) is defined by Eq. (5), where U_∞ is the average velocity in the x-direction and u' are the velocity fluctuations around the average in the same direction. Tu was measured using a 2.5 μm wire diameter single hot wire anemometer, at the average flow velocity of 18 ms^{-1}. At each position, data were evaluated from 4.8×10^5 samples taken during 2 min. For each of the five x-positions investigated, Tu were averaged from measurements at four positions in the y, z plane.

$$Tu = \frac{\sqrt{\overline{u'^2}}}{U} \tag{5}$$

Tu measured in configuration (B), without any cylinder in the test section, can be seen in Fig. 2. It was found to decay downstream from the grid, and was found to be $Tu = 6.7\%$ at $x = 0.000$ m.

2.6. Data analysis

The surface temperatures were evaluated from a $0.05D$ wide band of the TLC along the f–a–b–c–d line on the cylinder (Fig. 1). The symmetry in the measured temperatures for the front surface, from the center and towards the edge, along a–b and along a–f, was investigated for the configurations (A), (B), (C) and (D), and is shown in Fig. 3. Since each pair of such curves is nearly

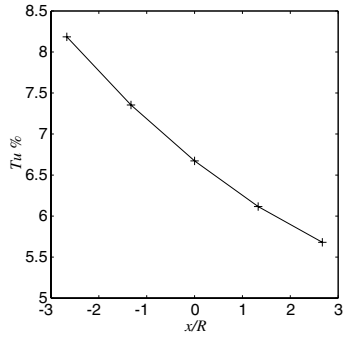

Fig. 2. Measured turbulence intensity downstream of the turbulence generating grid used in configuration (B), without any cylinder in the test section at $U_\infty = 18$ ms^{-1}.

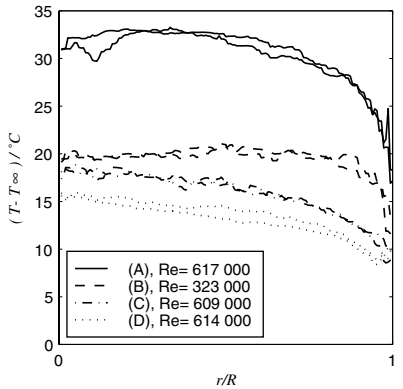

Fig. 3. Examination of symmetry in the measured temperatures on the front (upstream) cylinder surface for the cylinder in different configurations (A), (B), (C), (D): in each pair of temperature profiles for the same Re, one is along line a–b and the other along a–f (Before data smoothing).

[3] The MathWorks, 3 Apple Hill Drive, Natick, MA 01760-2098.

identical, within the error range for the measurements, symmetry of the measurements is confirmed.

The temperatures were then smoothed along f–a–b–c–d by averaging over each ±8 adjacent value (±0.0267D), and new temperatures along a–b were calculated as averages of the data along a–b and a–f. Based on these temperatures (900 values along a–b–c–d) the coefficient h was calculated using Eq. (4), and further expressed in terms of a local Nusselt number Nu, defined by Eq. (3). Area-weighted averages $\overline{Nu}$ were calculated along a–b, b–c, c–d, and a–d, assuming that the local Nu was symmetrical around the cylinder axis.

The Nusselt number was correlated with the Reynolds number Re as,

$$Nu = CRe^{e} \tag{6}$$

where C and the exponent e were unknown constants to be determined from the measurements.

Nu was measured at three different Re, and C and e were calculated by finding the value of e which minimized the relative differences in C for these three Re. It is noteworthy that a more complete correlation for Nu would also include the Prandtl number, and for the flow stagnation region even the turbulence intensity level (cf. [12], Chapter 11). Since air was used in this study having a nearly-constant Prandtl number, and the turbulence intensity was only one of two values, these dependencies weren't included in Eq. (6).

A non-uniformity criterion for the variation in Nu along the cylinder surface a–d, was calculated by means of the surface-weighted relative standard deviation σ_{Nu}, defined by Eq. (7).

$$\sigma_{Nu} = \frac{\left[\frac{\sum (Nu_i - \overline{Nu}_{\text{a–d}})^2 A_i}{\sum A_i}\right]^{\frac{1}{2}}}{\overline{Nu}_{\text{a–d}}} \tag{7}$$

where, A_i was a small area of the cylinder, and Nu_i the Nusselt number valid for that area.

Another non-uniformity criterion that expresses the extreme relative differences in Nu along a–d was calculated as defined by Eq. (8), where $Nu_{\max}$ and $Nu_{\min}$ are the largest and smallest values of Nu along a–d, respectively.

$$\sigma_{\max} = \frac{Nu_{\max} - Nu_{\min}}{\overline{Nu}_{\text{a–d}}} \tag{8}$$

2.7. Error estimates

Based on error analysis, the error in the local Nu was estimated to be ±7%, in which the main source of error is in the TLC-measured surface temperatures. The error in the Reynolds number was estimated to be ±2%.

2.8. TLC-based visualization of the flow along the cylinder

Based on the fact that the convective heat transfer coefficients have a close relation to the nature of the flow along the surface, we developed a flow visualization device based on TLC. A 300 mm long and 2.5 mm thick smooth Plexiglas plate was constructed to allow TLC temperature measurements over one of its faces. The plate was aligned with the cylinder axis and perpendicular to the cylinder surface, see Fig. 4. The front (upstream) plate edge was rounded and its lower edge was held ≈1 mm above the cylinder surface. An electrically heated foil, 300 × 83 mm (Inconel on Kapton, of the same type as used on the cylinder) was bonded, with the Inconel side of the foil, to one of the plate faces.

The foil was spray-coated with black paint and then with a film of the TLC R35C20. A thermocouple was also bonded on the foil, and used for in situ calibrations of the TLC, before and after the measurements. The measured surface temperatures were median filtered over a square in size $0.1 \times 0.1R$ (14 × 14 image pixels). Data closer than $0.05R$ from the foil edges were therefore canceled. The non-uniformity over the surface in the measured temperatures was found to be within ±0.6 °C.

Measurements were performed on the plate: in configuration (A) at $Re = 1.75 \times 10^5$ and with the plate front edge at $xR^{-1} = -0.50, 0.00, 0.13, 0.50, 1.00, 1.50, 2.00$, and in configuration (B) and (C), with the plate front edge at $xR^{-1} = 0.00$. No plate was inserted into the flow during any heating of the cylinder.

The lowest temperature appearing on the surface (highest heat transfer coefficient) was identified for each x-position along the plate, creating a curve on the surface, and its significance is discussed in Section 3 below.

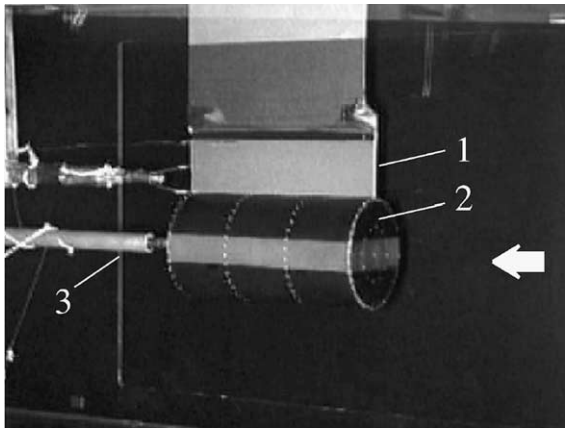

Fig. 4. The cylinder inside the test section, with the flow visualization plate mounted above its surface. (1) The plate, (2) the cylinder, (3) the cylinder support.

3. Experimental results

3.1. Measurements in configuration (A)

Measurements of the local Nusselt number (Nu) were performed on the cylinder in configuration (A) without any turbulence generators upstream of the cylinder, at the low upstream turbulence levels ($Tu < 0.1\%$), and at Reynolds numbers (Re) of 6.17×10^5, 3.22×10^5 and 1.77×10^5. Nu along the cylinder surface is shown in Fig. 5 and is seen to increase with Re, as expected, and the characteristic shape of the curves is similar for all Re. The average along the surface a–d, was for these three Re found to be, $\overline{Nu}_{a-d} = 990$, 640 and 430, respectively.

Nu is significantly higher along the surface b–c than on a–b, increasing from the front edge by at least two-fold to a maximal value at $xR^{-1} = 3.0$. On the downstream (rear) surface c–d, Nu drops to about half the previous values, increasing from the edge to the surface center. The latter behavior can be explained by the thermal consequences of wake formation on the downstream (rear) surface.

Using the tufts, it was found that flow reattachment along the cylinder surface b–c took place between $xR^{-1} = 2.93$ and 3.07, at $Re = 1.75 \times 10^5$. This coincides with the position measured for the maximal Nu along the same surface, and is only somewhat shorter than the reattachment length of $xR^{-1} = 3.18$–3.22 determined in [16] for Re and Tu similar to what was used here for a cylinder of $LD^{-1} = 10$ and measured in terms of reverse flow intermittence (reverse-flow time = 0.5). These results indicates that the cylinder used in our study was long enough to make the flow in the separated region independent of further increase in the cylinder length.

The temperature field on the heated and TLC-coated plate mounted above the cylinder surface b–c, with the plate upstream edge at $xR^{-1} = 0.0$, is shown in Fig. 6. The thick line in the figure shows the location of the minimal temperatures on the plate, which, as discussed above, coincides with the maximal convective heat transfer coefficient (h). It starts at the leading edge of the cylinder (position b), follows a curved path through a maximal height of $yR^{-1} = 0.5$ and descends to reach the cylinder surface at about $xR^{-1} = 3$, which is in the above-mentioned flow reattachment region to the cylinder.

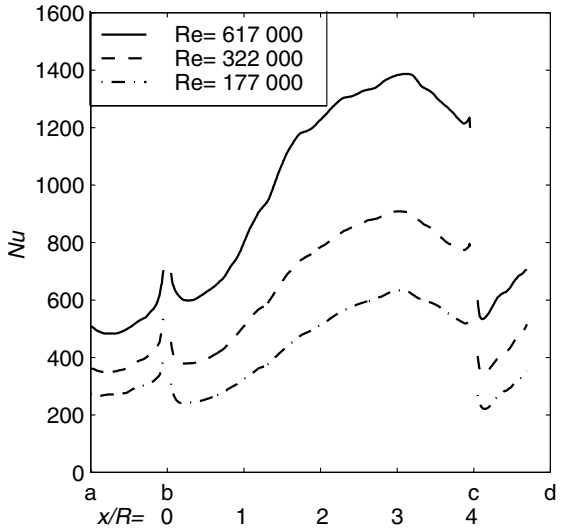

Fig. 5. The Nusselt numbers along the cylinder surfaces, configuration (A), for different Re.

Velocities measured above a longer cylinder in an axial flow of $Re = 5.62 \times 10^4$, by Ota [17], showed that the dividing stream line for the separated region was similar in shape and position to the line on the plate that traces our measured loci of maximal convection heat transfer, see Fig. 7. A plausible reason may be that the maximal convective heat transfer occurs at the fluctuating (turbulent) free shear layer. Outside the separated region there is the laminar main flow, and inside the separated region, a flow of lower velocity is expected, which in both

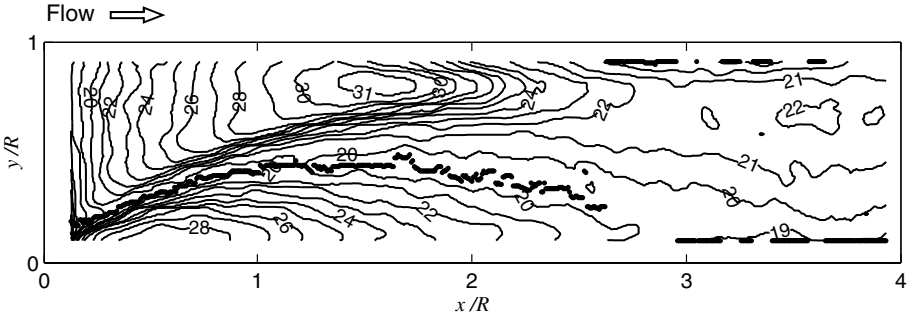

Fig. 6. Isotherms $T - T_\infty$ °C, on the flow visualization plate mounted above the cylinder in configuration (A), $Re = 1.75 \times 10^5$, $Tu < 0.1\%$. The minimal temperature locations are marked by the bold black dots.

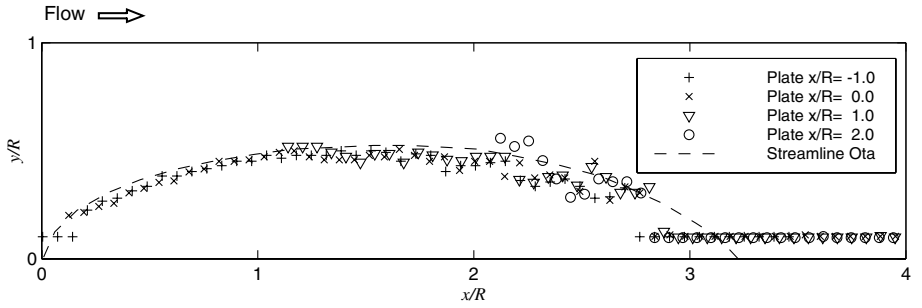

Fig. 7. The minimum temperature curves found on the flow visualization plate, with the plate upstream edge positioned at different x-locations, for the cylinder in flow configuration (A) and $Re = 1.75 \times 10^5$. Included is a measured average dividing streamline at $Re = 5.62 \times 10^4$ [17].

cases may induce a lower convection heat transfer on the plate, than the free shear layer does.

A test was performed to examine the sensitivity of the results to the x-position of the plate. The plate front edge was set at four different x-positions, in the range $-1.0 \leqslant xR^{-1} \leqslant 2.0$, and the loci of the minimal temperature on the plate are shown in Fig. 7. No significant variations were seen in the position of the minimum temperature loci relative to the cylinder.

In other tests, performed at higher Re, the situation was different. The points of maximum heat transfer did not all fall on one line, probably because of transition to turbulence in the boundary layer on the plate outside of the separated region. Such transition to turbulence on a flat plate in flow parallel to its surface, is known to be induced by, (1) high Re^* (where Re^* in this case is based on the distance from the leading edge), (2) turbulence in the free stream, (3) surface roughness on the plate, and (4) possibly also by the shape of the leading edge. A smooth flat plate has a stable laminar boundary layer for $Re^* < 10^5$, while transition is more easily induced by disturbances for higher Re^*, and difficult to prevent for $Re^* > 2 \times 10^6$ [20]. Therefore, for the present measurement on the plate, which was performed at $Re = 1.75 \times 10^5$, the boundary layer on rear part was expected to be unstable.

We conclude in the present tests on the flat plate and at the lower velocity (probably as long as the boundary layer on the plate outside the separated region remains laminar), that the minimum temperature curves would indicate the extent of the separated flow region, while this indication may be less clear for flows producing a turbulent boundary layer on the plate outside the separated region.

Nu along the cylinder front surface a–b in configuration (A), was extrapolated using the local constant e (Fig. 8), to $Re = 4.2 \times 10^4$, for comparison with results from a study by Sparrow and Geiger [13] that used the naphthalene sublimation mass-heat transfer analogy technique at that Re, and the results are shown in

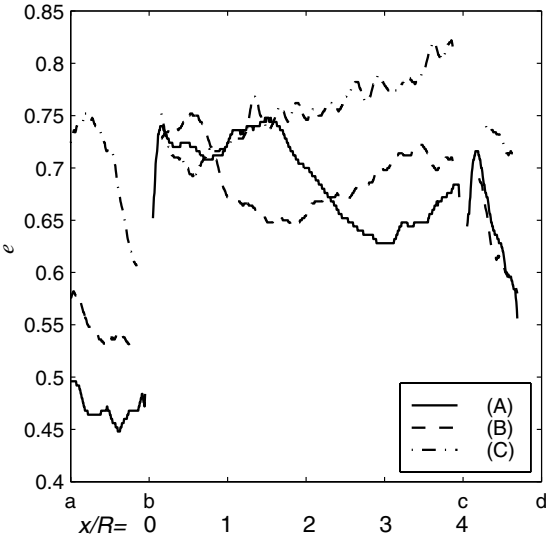

Fig. 8. The calculated local exponents e of Eq. (6) along the cylinder surfaces, for the flow configurations (A), (B) and (C).

Fig. 9. At position (a) our values are 10% lower, and near the corner position (b) 25% lower than theirs. This trend of increasing difference is expected because of the different surface boundary conditions used, where their surface of uniform naphthalene vapor density is analogous to a uniform wall temperature and not to the constant heat flux surface used in our study. On a constant heat flux surface on which h increases in the flow direction, a downstream location will have a temperature lower than an upstream position, and therefore cause lower h at that downstream position.

The higher values of Nu at the stagnation region position (a) by Sparrow and Geiger is in part expected due to the higher free stream turbulence $Tu = 0.5\%$, which can be compared to $Tu < 0.1\%$, in our study. The

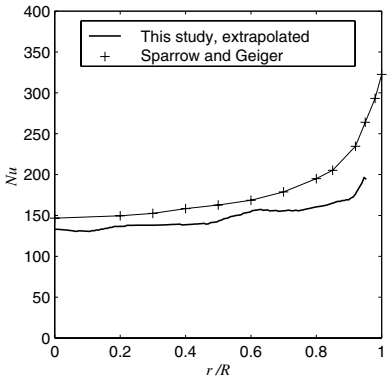

Fig. 9. *Nu* along the cylinder front surface a–b in configuration (A), extrapolated, (using the local *e* of this study, to the $Re = 4.2 \times 10^4$ in the study by Sparrow and Geiger [13], for comparison with their results.

extrapolation of *Nu* to the lower *Re* used by Sparrow and Geiger, introduces uncertainty in our *Nu* values.

The measured *Nu* along the cylinder surface b–c for configuration (A) was extrapolated, using the local constant *e* (Fig. 8), to the lower $Re = 5.36 \times 10^4$ used in the experiment by Ota and Kon [14]. Ota and Kon performed the measurements on a long cylinder of $LD^{-1} = 13$ having a constant heat flux surface, in a flow of $Tu = 0.8\%$. The comparison between there results and ours are shown in Fig. 10, and they are in good agreement despite the 10-fold lower *Re*. It is also seen that the large difference in cylinder length does not have a significant influence on *Nu* in this case, as was discussed above in relation to the size of the separated region.

The above-described agreement between our results and those of [13,14,16,17], gives further credibility to the results.

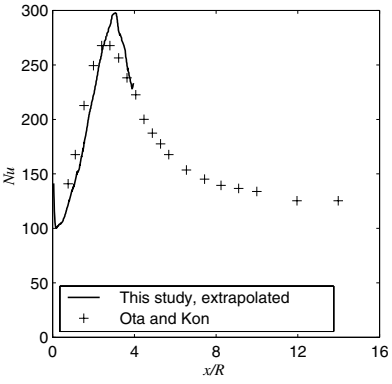

Fig. 10. *Nu* along the cylinder surface b–c in configuration (A), extrapolated (using the found local *e*) to the $Re = 5.36 \times 10^4$ in the study by Ota and Kon [14], for comparison with their results.

3.2. Measurements in configuration (B)

A turbulence-generating grid was inserted upstream of the cylinder, Fig. 1, generating a free stream turbulence intensity, *Tu*, of 6.7%, and the experiments were conducted at Reynolds numbers of 3.23×10^5, 1.77×10^5, and 8.9×10^4. The Nusselt number distribution along the cylinder surface is shown in Fig. 11. *Nu* is seen to increase with *Re*, as expected, and the characteristic shape of the curves is similar for all *Re*.

On the front (upstream) surface of the cylinder, a–b, *Nu* maintains a nearly constant value, different for each *Re*. Compared with the results for $Tu < 0.1\%$ (Fig. 5), it shows that the increase of *Tu* to 6.7% at $Re = 3.23 \times 10^5$ caused this uniformity of *Nu*, as well as an increase of 42% in the $\overline{Nu}_{a-b}$.

The increase in *Nu* due to the increase in turbulence is similar in magnitude to that found on the front of a circular cylinder in cross-flow [8]. The results are consistent with the knowledge that increase in free stream turbulence increases the convective heat transfer coefficient magnitude and its uniformity.

The average $\overline{Nu}_{b-c}$, is significantly higher than on the front surface $\overline{Nu}_{a-b}$ and a maximum in *Nu* appear at $xR^{-1} = 1.8$. The flow reattachment, as determined by the tufts, appeared downstream of the maximum convection heat transfer and in between $xR^{-1} = 2.00$ and 2.26.

The temperature field on the flow visualization plate mounted above surface b–c, for this configuration (B), is shown in Fig. 12. The extent of the separated region is smaller than it was for the cylinder in configuration (A), and the curve of minimum temperature has a maximal height of $yR^{-1} = 0.3$ at about $xR^{-1} = 1$. Its extrapolation meets the cylinder surface at $xR^{-1} > 2$, which agrees with the mean flow reattachment on to the surface as measured using the tufts.

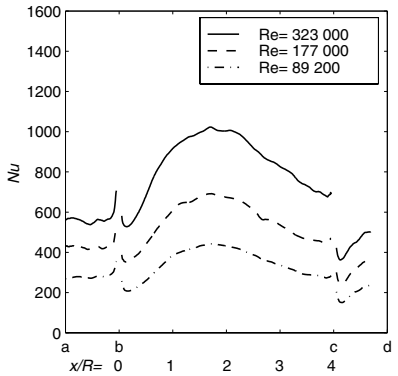

Fig. 11. Nusselt numbers along the cylinder surface, from the measurements in axial flows with free stream turbulence $Tu = 6.7\%$, configuration (B), for different *Re*.

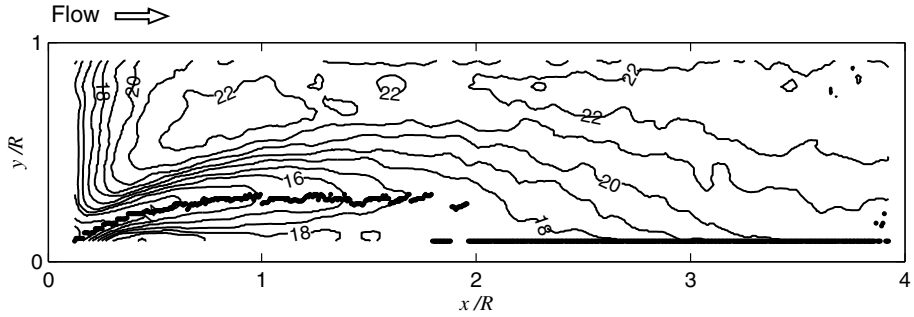

Fig. 12. Isotherms, $T - T_\infty$ °C, on the flow visualization plate mounted above the cylinder in configuration (B), $Re = 1.75 \times 10^5$, $Tu = 6.7\%$. The minimal temperatures are marked with black dots.

On the rear surface c–d, *Nu* drops to a lower value, increasing from the cylinder edge towards its center. Along the whole surface a–d, the average of *Nu* for these three Reynolds numbers (3.23×10^5, 1.77×10^5 and 8.9×10^4) was found to be $\overline{Nu}_{a-d} = 780$, 520 and 330, respectively.

3.3. Measurements in configuration (C)

A (1/3)*D* diameter disk was placed upstream of the cylinder as detailed earlier for configuration (C), and measurements were performed on the cylinder at Reynolds numbers of $Re = 6.09 \times 10^5$, 3.23×10^5 and 1.77×10^5. The Nusselt number distribution along the cylinder surface is shown in Fig. 13a, where *Nu* is seen to increase with *Re*, as expected, and the characteristic shape of the curves is similar for all *Re*.

On the front (upstream) surface of the cylinder, along a–b, *Nu* increases from the cylinder center to its edge. On the surface b–c, a sharp maximum in *Nu* appear close to its upstream edge at position (b), with *Nu* decreasing to about half of the maximal value towards the rear edge at position (c).

The temperature field on the flow visualization plate mounted above surface b–c for this configuration (C) is shown in Fig. 14. The curve of minimum temperature, which was seen both in configurations (A) and (B), cannot be seen here, indicating a much smaller or non-existing separated region. A growing region of high convection heat transfer towards its rear can be seen on the plate, possibly related to growing turbulent flow structures along the cylinder.

On the rear surface c–d, *Nu* is lower, increasing from the cylinder edge towards its center. The average Nusselt number along the entire surface a–d, was for these three *Re* found to be $\overline{Nu}_{a-d} = 1220$, 790 and 490, respectively. Moving the disc closer to the cylinder, from 1.00*D* to 0.50*D* from the front surface, gave asymmetric values of *Nu* on the front surface f–a–b, and symmetry was re-established when the distance was again increased to 1.00*D*. Since heat transfer patterns follow closely the fluid mechanics, it is interesting to note that the drag coefficient for the disc and the cylinder front together was shown in [18] to change from 0.72 without any disc to 0.28 with a disc of the same diameter and at the same distance as of configuration (C).

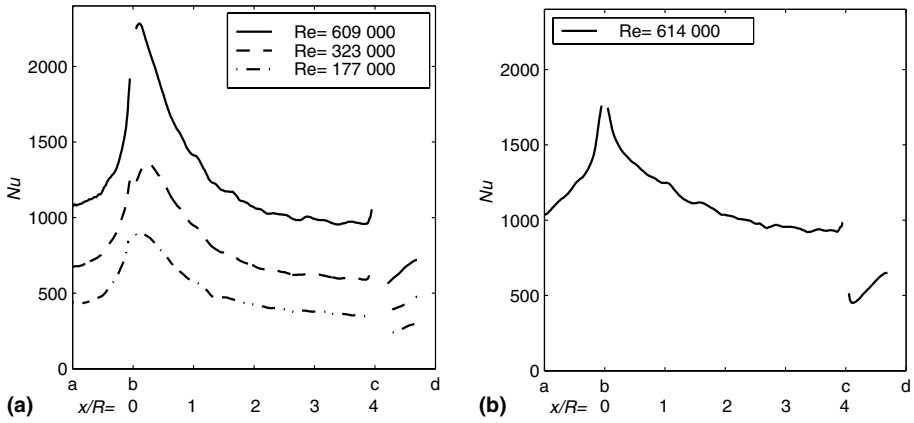

Fig. 13. *Nu* along the cylinder surface for different *Re* (a) with a (1/3)*D* diameter disk placed 1.00*D* upstream of the cylinder in configuration (C), (b) with a (2/3)*D* diameter disk placed 1.00*D* upstream of the cylinder in configuration (D).

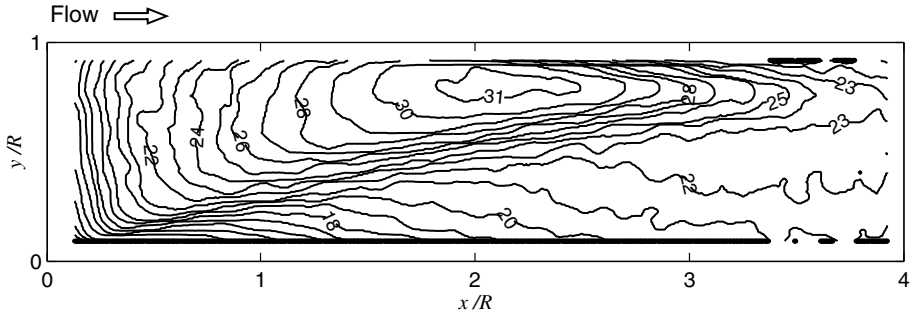

Fig. 14. Isotherms, $T - T_\infty$ °C, on the flow visualization plate mounted above the cylinder in configuration (C), $Re = 1.75 \times 10^5$.

The drag coefficient for a cylinder with rounded corners, which prevented development of any separated regions, was found to have the very small value of 0.01 [18]. Smallness of the separated region on surface b–c indicates therefore a small drag force on the cylinder front.

3.4. Measurements in configuration (D)

Here a disc twice as large as the previous one, of diameter (2/3)D, was placed upstream of the cylinder as detailed earlier for configuration (D), for $Re = 6.14 \times 10^5$. As shown in Fig. 13b, Nu is similar to that in configuration (C) at the same Re level. The main difference is the peak in Nu at the front edge (location b), which is lower, further confirmed by the lower $\overline{Nu}_{a\text{–}d} = 1080$.

On the downstream surface c–d, Nu was found to be very similar to that in configurations (A), (B), (C), which indicated a low sensitivity of Nu in the wake region to the different upstream flow conditions. The drag coefficient, for the disc and the cylinder front together, is expected to change from 0.72 while the disc is absent, to 0.2, using the disc in configuration (D), as was estimated from data for a similar configuration reported by Koenig and Roshko [18].

3.5. The dependence of Nu on Re

The observed similarity of the curves which describe the dependence of Nu on Re for all Reynolds numbers investigated here, Figs. 5, 11, and 13a, indicates that it may be possible to find a value of the power e that would describe the behavior of the local Nu with respect to Re shown in Eq. (6). These values, for all cylinder surfaces for the configurations (A), (B) and (C), were calculated and are shown in Fig. 8.

On the front surface a–b for configurations (A) and (B), it was found that e increased with an increase in Tu, while e was even larger when using the disc in configuration (C).

On the middle surface b–c, e had a minimum where Nu has a maximum. For configuration (A) the minimum in e was found at $xR^{-1} = 3.0$, for configuration (B) it was at $xR^{-1} = 1.8$, and for configuration (C) at $xR^{-1} = 0.55$. For all the configurations, e was found to increase with a similar slope from the minimum and towards point c. It is noteworthy that the use of the exponent $e = 0.75$ could collapse the local Nu on the long surface in the study by Ota and Kon [14] (see Introduction for details).

On the rear surface c–d, and for all of the configurations (A), (B) and (C), e was found to be somewhat lower than on the middle surface b–c, decreasing from the edge.

To obtain the average values of the Nusselt number, the local Nu were averaged, and C and e for the averages on surface a–b, b–c, c–d and the whole cylinder a–d, are shown in Table 1 for the three configurations (A), (B), (C). The exponent, which indicates the trends with Re of the average for the whole cylinder $Nu_{a\text{–}d}$ and for the configurations (A), (B), (C), was found to be in the range $0.67 < e_{a\text{–}d} < 0.73$.

A laminar boundary layer flow was expected to appear in configuration (A) on the front end surface, which occupies only 11% of the total cylinder surface and the exponent was found here to be at its lowest level $e_{a\text{–}b} = 0.46$. In a previous study [13] the naphthalene sublimation mass-heat transfer analogy technique was used and the exponent for the cylinder front was found to be $e = 0.5$. The relatively few Re levels used for the calculation of e in our study is a source of uncertainty, which may be an explanation to the differences found in the comparison.

Table 1
The constants C and e of Eq. (6) for the averages $\overline{Nu}_{a\text{–}b}$, $\overline{Nu}_{b\text{–}c}$, $\overline{Nu}_{c\text{–}d}$ and $\overline{Nu}_{a\text{–}d}$ and for the flow configurations (A), (B), and (C)

Configuration		a–b	b–c	c–d	a–d
(A)	C	1.088	0.122	0.096	0.134
	e	0.466	0.682	0.656	0.668
(B)	C	0.662	0.140	0.140	0.155
	e	0.534	0.686	0.632	0.674
(C)	C	0.162	0.058	0.055	0.070
	e	0.678	0.750	0.704	0.734

Table 2
The averages $\overline{Nu}_{a-d}$ and $\overline{h}_{a-d}$ and the non-uniformities in Nu for a typical gas quenching case of a 49 mm diameter, 98 mm long cylinder in 20 ms^{-1} axial flow of nitrogen quenchant at 10 bar, 300 K

Configuration	$\overline{Nu}_{a-d}$	$\overline{h}_{a-d}$	σ_{Nu}	σ_{max}
(A)	990	540	0.32	0.89
(B)	1240	680	0.24	0.78
(C)	1240	680	0.31	1.42
(D)	1080	590	0.24	1.2

3.6. An example of practical consequence for axial flow gas cooling of an $LD^{-1} = 2$ cylinder

As stated in the introduction, gas quenching of steel is improved with the magnitude and uniformity of the convection heat transfer coefficients (h). A comparison between the configurations (A), (B), (C) and (D) was performed, for a representative example: nitrogen gas quenchant at 10 bar, 300 K and a flow velocity of 20 ms^{-1}. A cylinder of 49 mm diameter will produce for this flow a $Re = 6.14 \times 10^5$.

The average $\overline{Nu}_{a-d}$ were calculated using Eq. (6), with the coefficients C and e found in this study (Table 1). $\overline{h}_{a-d}$ was then evaluated from Eq. (3) and the results are presented in Table 2. For this comparison, Nu were for configurations (B) extrapolated to the higher Re of interest. The coefficient $\overline{h}_{a-d}$ was in configuration (B) found to be 25%, in (C) 26%, and in (D) 10% higher than in configuration (A) with the undisturbed free stream.

The non-uniformity in Nu (and h) σ_{Nu} was found, compared to configuration (A), to be lower by 26% in configuration (B), by 26% in configuration (D), and by very little in configuration (C). The second non-uniformity number σ_{max} confirms that configuration (B) has the lowest non-uniformity in Nu.

Configuration (B) thus generated the highest average $\overline{h}_{a-d}$ at also a low non-uniformity σ_{Nu} and σ_{max}, and may therefore be the best choice for quenching. The upstream turbulence-generation grid will generate an undesirable pressure drop, but a possible solution to this problem could be to use a grid, or another smaller device for disturbing the flow, just locally in front of the cylinder, which can generate a similar effect at a lower pressure drop. It should also be noted that high levels of upstream turbulence will exist anyway in commercial quench chambers, due to effects of the fan and the flow geometry.

4. Conclusions

The local Nusselt number (Nu) distributions on all surfaces of a two-diameter long cylinder were measured in axial flows of air, at Reynolds numbers (Re) of 8.9×10^4–6.17×10^5 (9–63 ms^{-1}), by using thermochromic liquid crystals (TLC) on thin foils that produced a constant surface heat flux.

Different upstream air flow conditions were examined, set by varying the flow turbulence level (Tu), by the use of a turbulence generating grid, and by using flow modification inserts that were circular discs of two sizes, in front of the cylinder. These and the grid were found to create a major change in the magnitude and distribution of the local Nu on the cylinder.

Nu was found to increase with the Re, but at different amounts for different locations on the cylinder. Correlations in the form $Nu = CRe^e$ were developed and presented for the average of Nu over the three different cylinder surfaces a–b, b–c, c–d and over the whole cylinder a–d, and the local exponent e was calculated along the whole cylinder.

Increase of the turbulence intensity (Tu) from <0.1% to 6.7% at the same $Re = 6.14 \times 10^5$, increased the average Nusselt number over the cylinder by 25%, and decreased the Nu non-uniformities (σ_{Nu} and σ_{max}) by 26% and 12%, respectively. For the same Re, the largest flow modification insert (a circular disc in front of the cylinder) increased $\overline{Nu}_{a-d}$ by 10% and reduced σ_{Nu} by up to 25%, but increased σ_{max} by 33%.

A TLC-coated heated flat plate mounted in the flow above the cylinder was demonstrated to help visualize the flow field above the cylinder. The temperature field on the plate was affected by the flow, and a track of minimal temperatures (maximal h) appeared on the plate, which was for configuration (A) shown to be the same as the envelope of the separated flow region above the cylinder, i.e. the dividing stream line, measured in a past study [17].

The location of flow reattachment on the cylinder curved surface was measured using tufts, and was for configuration (A) found similar to the location of the maximum in Nu. For configuration (B) the maximum in Nu was found within the separated region.

Our results agree well with the small amount of data published by others, when extrapolated to their conditions.

Acknowledgments

This work was partially supported by AGA AB (now Linde Gas) and Ipsen International GmbH. Marcus Gällstedt and Ulf Landen are acknowledged for valuable help with the experimental equipment. Ulf Andersson at Calesco foil AB is acknowledged for his constructive cooperation in the design and manufacturing of the foil.

References

[1] M. Lind, N. Lior, F. Alavyoon, F. Bark, Flows effects and modeling in gas-cooled quenching, in: Proc. Heat Transfer 1998, 11th International Heat Transfer Conference, Kyongju, Korea, vol. 3, 1998, pp. 171–176.

[2] A. Thuvander, A. Melander, M. Lind, N. Lior, F. Bark, Prediction of convective heat transfer coefficients and their effects on distortion and mechanical properties of cylindrical steel bodies quenched by gas cooling, in: 5th ASME/JSME Joint Thermal Engineering Conference, San Diego, paper AJTE99-6289, 1999, pp. 171–176.

[3] R. Wiberg, B. Muhammad-Klingmann, J. Ferrari, N. Lior, Use of thermochromic coatings for the experimental determination of the distribution of heat transfer coefficients in gas-cooled quenching, in: Proc. 5th ASM Heat Transfer and Surface Eng. Conf. in Europe, Gothenburg, Sweden, 2000, pp. 275–286.

[4] R. Wiberg, N. Lior, Error causes and magnitudes in thermochromic liquid crystals thermometry, in: IMECE'03, 2003 ASME International Mechanical Engineering Congress and Exposition Washington, DC, USA, paper IMECE 2003-42101, 2003, pp. 15–21.

[5] J. Ferrari, N. Lior, J. Slycke, An evaluation of gas quenching of steel rings by multiple-jet impingement, J. Mater. Process. Technol. 136 (2003) 190–201.

[6] M. Vynnycky, J. Ferrari, N. Lior, Some analytical and numerical solutions to inverse problems applied to phase-transformation tracking gas quenching, J. Heat Transfer 125 (1) (2003) 1–10.

[7] N. Lior, The cooling process in gas quenching, invited keynote presentation and paper, Proceedings of International Conference on Advances in Materials and Processing Technology, vol. 1, AMPT, Dublin, Ireland, 2003, pp. 171–179.

[8] G.W. Lowery, R.I. Vachon, The effect of turbulence on heat transfer from heated cylinders, Int. J. Heat Mass Transfer 18 (1975) 1229–1242.

[9] E. Achenbach, Total and local heat transfer from a smooth circular cylinder in cross-flow at high reynolds number, Int. J. Heat Mass Transfer 18 (1975) 1387–1396.

[10] M.M. Zdravkovic (Ed.), Flow around circular cylinders, Fundamentals, vol. 1, Oxford Science Publications, Oxford University Press Inc., Oxford, 1997.

[11] E. Achenbach, Heat transfer from a staggered tube bundle in cross-flow at high Reynolds numbers, Int. J. Heat Mass Transfer 32 (2) (1989) 271–280.

[12] A. Zukauskas, High-performance Single-phase Heat Exchangers, Hemisphere Pub., New York, 1989.

[13] E.M. Sparrow, G.T. Geiger, Local and average heat-transfer characteristics for a disk situated perpendicular to a uniform-flow, J. Heat Transfer 107 (2) (1985) 321–326.

[14] T. Ota, N. Kon, Heat transfer in an axisymmetric separated and reattached flow over a longitudinal blunt circular cylinder, J. Heat Transfer (1977) 155–157.

[15] E.M. Sparrow, S.S. Kang, W. Chuck, Relation between the points of flow reattachment and maximum heat-transfer for regions of flow separation, Int. J. Heat Mass Transfer 30 (7) (1987) 1237–1246.

[16] M. Kiya, O. Mochizuki, H. Tamura, T. Nozawa, R. Ishikawa, K. Kushioka, Turbulence properties of an axisymmetric separation-and-reattaching flow, AIAA J. 29 (6) (1991) 936–941.

[17] T. Ota, An axisymmetric separated and reattached flow on a longitudinal blunt circular cylinder, J. Appl. Mech. (1975) 311–314.

[18] K. Koenig, A. Roshko, An experimental-study of geometrical effects on the drag and flow field of 2 bluff-bodies separated by a gap, J. Fluid Mech. 156 (1985) 167–204.

[19] B. Lindgren, A.V. Johansson, Evaluation of the flow quality in the mtl wind-tunnel, Technical report TRITA-MEK report 2002:13, Department of Mechanics, KTH, 2002.

[20] B. Massey, Mechanics of Fluids, seventh ed., Stanley Thornes Publishers Ltd, Berlin, 1998, Chapter 8, pp. 314–315.